SCIENCE CHINA
Physics, Mechanics & Astronomy

• Article •

February 2024 Vol. 67 No. 2: 220312
https://doi.org/10.1007/s11433-023-2259-1

Experimental observation of spontaneous symmetry breaking in a quantum phase transition

Wen Ning[1†], Ri-Hua Zheng[1†*], Jia-Hao Lü[1], Fan Wu[1], Zhen-Biao Yang[1,2*], and Shi-Biao Zheng[1,2*]

[1] *Fujian Key Laboratory of Quantum Information and Quantum Optics, College of Physics and Information Engineering, Fuzhou University, Fuzhou 350108, China;*
[2] *Hefei National Laboratory, Hefei 230088, China*

Received July 11, 2023; accepted October 18, 2023; published online January 5, 2024

Spontaneous symmetry breaking (SSB) plays a central role in understanding a large variety of phenomena associated with phase transitions, such as superfluid and superconductivity. So far, the transition from a symmetric vacuum to a macroscopically ordered phase has been substantially explored. The process bridging these two distinct phases is critical to understanding how a classical world emerges from a quantum phase transition, but so far remains unexplored in experiment. We here report an experimental demonstration of such a process with a quantum Rabi model engineered with a superconducting circuit. We move the system from the normal phase to the superradiant phase featuring two symmetry-breaking field components, one of which is observed to emerge as the classical reality. The results demonstrate that the environment-induced decoherence plays a critical role in the SSB.

quantum phase transition, Rabi model, spontaneous symmetry breaking, superconducting circuit, Schrödinger cat states

PACS number(s): 03.65.Ud, 03.67.-a, 42.50.Pq

Citation: W. Ning, R.-H. Zheng, J.-H. Lü, F. Wu, Z.-B. Yang, and S.-B. Zheng, Experimental observation of spontaneous symmetry breaking in a quantum phase transition, Sci. China-Phys. Mech. Astron. **67**, 220312 (2024), https://doi.org/10.1007/s11433-023-2259-1

1 Introduction

The concept of spontaneous symmetry breaking (SSB) has infiltrated almost all research branches of modern physics, ranging from condensed physics [1] to quantum field theory [2, 3]. SSB appears when the observed systems lack the symmetry of the governing physical laws. It underlies phase transitions described by the Ginzburg-Landau-Wilson paradigm, e.g., Bardeen-Cooper-Schrieffer superconducting phenomena [4], and is critical to the Higgs mechanism [5], where the mass is generated by breaking the invariance associated with the Lagrangian. Besides these, SSB plays an important role in the evolution of biology, e.g., the visual cortex processes image by spontaneously breaking both the translation and rotation symmetries, which was recently interpreted in terms of zero-temperature phase transitions [6]. In a more general sense, SSB is responsible for the formation of the universe [7], and thus gives arise to the infinite diversity of nature.

In quantum field theory, SSB occurs in an infinitely extended system that possesses degenerate vacua. In this case, an infinitesimal perturbation is sufficient to single out one of these vacua as the real ground state. For a quantum system with a definite size, the symmetry is generally broken by the decoherence process [8-10], where the environment

*Corresponding authors (Ri-Hua Zheng, email: ruazheng@gmail.com; Zhen-Biao Yang, email: zbyang@fzu.edu.cn; Shi-Biao Zheng, email: fjqiqo@fzu.edu.cn)
† These authors contributed equally to this work.

or a monitoring meter continuously gathers the information about the system by entangling its state with the system. This process progressively destroys the quantum coherence between the symmetrically superposed quasiclassical components with broken symmetry, transforming the quantum superposition into a classical mixture [11]. The decoherence rate linearly scales with the size of the system, which prohibits observation of quantum superpositions in a macroscopic object, such as the famous Schrödinger cat [12]. In this case, the environment or meter plays a central role in the symmetry breaking of the observed system.

Despite impressive experimental demonstrations in classical systems [13-17], observations of the SSB associated with quantum phase transitions have remained an outstanding task. As the energy gap vanishes at the critical point, an adiabatic evolution across this point would require an infinitely long time. For this reason, experimental demonstrations of quantum phase transitions have been focused on out-of-equilibrium systems [18-34], where transitions between distinct phases were realized by a quenching process or in a dynamical manner. In thus-realized superradiant phase transitions (SPTs) with an ultracold atomic gas trapped in an optical cavity, the breaking of both discrete [30] and continuous translation symmetries [31, 32] have been observed. However, in these experiments, the symmetries were not broken spontaneously, but explicitly with a small symmetry-breaking field or by a detuning that broke the Hamiltonian symmetry. In two very recent experiments, continuous symmetry-breaking phases were prepared in a one-dimensional ionic chain [35] and a two-dimensional Rydberg array [36], respectively. Despite these impressive progresses, it remains an experimental challenge to directly observe how the SSB occurs during a quantum phase transition, which is responsible for the emergence of a classical, symmetry-breaking state under a symmetric Hamiltonian.

2 Physical model and theoretical predictions

We here report an experimental observation of such a process in an effective Rabi model, engineered in a circuit quantum electrodynamics (QED) architecture. With the high level of control over the effective coupling between the qubit and the photonic field involved in the Rabi Hamiltonian, we realize a second-order SPT, where the system is moved from a normal phase (NP) to a superradiant phase (SP) formed by two coherent field states correlated to different qubit states. We observe the progressive evolution of the field from the initial symmetric vacuum to two superposed components, each of which has a broken symmetry in phase space, and the transition of their symmetric superposition to a classical mixture during their growth. Our results reveal that SSB is closely related to a quantum natural selection made by the environment [37], which continuously performs measurements on the system but with inaccessible records, washing the quantum coherence between the two quasi-classical components emerging from a quantum phase transition.

The system under investigation is comprised of a qubit and a photonic field, coupled by the Rabi Hamiltonian [38, 39]

$$H_{RM} = \delta a^{\dagger} a + \frac{1}{2}\Omega\sigma_z + \frac{1}{2}\lambda\sigma_x(a^{\dagger} + a). \tag{1}$$

Here $a^{\dagger}$ and a denote the creation and annihilation operators for the photonic field with a frequency δ, $\sigma_x = |e\rangle\langle g| + |g\rangle\langle e|$ and $\sigma_z = |e\rangle\langle e| - |g\rangle\langle g|$ are pseudo-spin operators for the qubit, which has a frequency Ω, and whose upper and lower levels are denoted as $|e\rangle$ and $|g\rangle$. The qubit-resonator coupling strength is λ. The Rabi Hamiltonian is invariant under the parity transformation $(-1)^{a^{\dagger}a+|e\rangle\langle e|}$, featuring a Z_2 symmetry. In the limit $\Omega/\delta \to \infty$, the system has a unique ground state below the critical point $\xi = \lambda/\sqrt{\Omega\delta} = 1$, given by $\left|\psi_{np}\right\rangle = S(r_{np})|0\rangle|g\rangle$, where $S(r_{np})$ is a squeezing operator with $r_{np} = -\frac{1}{4}\ln(1-\xi^2)$. Due to the limited frequency ratio Ω/δ in a real experiment, when $\xi < 1$, the field in the experimentally realized Rabi model almost remains in the vacuum state, which is significantly distinct from the ideal ground state for $\Omega/\delta \to \infty$. Above the critical point, the system enters the SP, characterized by two degenerate ground states $\left|\psi_{sp}^{\pm}\right\rangle = D(\pm\alpha)S(r_{sp})|0\rangle|\pm\rangle$, where $r_{sp} = -\frac{1}{4}\ln(1-\xi^{-4})$, $D(\alpha) = \exp[\alpha(a^{\dagger} - a)]$ with $\alpha = \sqrt{\frac{\Omega}{4\xi^2\delta}(\xi^4 - 1)}$, and $|\pm\rangle$ are two qubit basis states. Compared with the case in the Dicke model, the SPT in the Rabi mode is realized by replacing thermodynamical limit with the scaling limit, where the frequency ratio between qubit and the field tends to infinity [39]. Each of these ground states is symmetry-broken, signified by the nonvanishing coherence $\left\langle\psi_{sp}^{\pm}\right| a \left|\psi_{sp}^{\pm}\right\rangle = \pm\alpha$ [39]. Under unitary Hamiltonian dynamics, adiabatically increasing the parameter ξ across the critical point would evolve the system to the equal superposition of the two degenerate ground states

$$|\psi_e\rangle = N_e\left(\left|\psi_{sp}^{+}\right\rangle + \left|\psi_{sp}^{-}\right\rangle\right), \tag{2}$$

which preserves the parity of the ground state below the critical point. However, during the evolution, the system is inevitably coupled to the environment, which continuously monitors the system in the preferred basis [11], forcing the system to choose between these two conflicting classical states.

3 Device and experimental scheme

The experiment is performed with a circuit QED device, which involves a resonator of a fixed frequency $\omega_r/2\pi$ = 5.581 GHz controllably coupled to 5 frequency-tunable Xmon qubits, with an on-resonance coupling strength of $g/2\pi \simeq 20$ MHz. One of these qubits is used as the test qubit for realizing the Rabi model, while the other qubits are effectively decoupled from the resonator during the quenching process due to the large detunings. The experiment starts by tuning the test qubit to the frequency $\omega_q/2\pi = 5.21$ GHz, where it is subjected to a transverse microwave driving of an amplitude $A = 2\pi \times 15$ MHz and two longitudinal parametric modulations, one having a fixed frequency $\nu_1/2\pi$ = 185 MHz and amplitude $\varepsilon_1 = 2\pi \times 146$ MHz, while the other bearing a fixed frequency $\nu_2/2\pi = 25.97$ MHz but a tunable amplitude ε_2. With this setting, the qubit is coupled to the transverse field at the carrier and to the resonator at the second upper sideband with respect to the first modulation [22]. In the framework coinciding with the Rabi precession associated with the transverse drive and discarding the fast rotating terms, the system dynamics can be described by the effective Rabi Hamiltonian with an effective coupling strength $\lambda = gJ_2(\mu)/2 = 2\pi \times 0.735$ MHz, where $J_n(\mu)$ is the nth Bessel function of the first kind with $\mu = \varepsilon_1/\nu_1$. The effective qubit frequency and resonator frequency are $\Omega = \varepsilon_2/2$ and $\delta = \omega_r - \omega_q - 2\nu_1$, respectively. The quench parameter ξ is controllable by adjusting the amplitude ε_2 of the second parametric modulation and by tuning the Stark shift of the resonator produced by an ancilla qubit dispersively coupled to the resonator.

The quench parameter ξ is modeled as a linear function of time, $\xi = 0.5 + 2t/(3\ \mu\text{s})$. We first investigate the evolution of the resonator irrespective of the qubit state. To monitor the real-time evolution of the resonator, after a preset quench time t we switch off both the transverse and longitudinal drives, decoupling the test qubit from the resonator. Then the Wigner tomography of the resonator's state is performed by applying a microwave pulse to the resonator to produce a displacement operation $D(-\beta)$, tuning an ancilla qubit on resonance with the resonator for a given time, and then biasing it back to its idle frequency for state readout. The Wigner function and the reduced density operator ρ_r for the resonator can be extracted from the recorded Rabi oscillations signals of the ancilla qubit.

4 Loss-induced SSB

The classical characteristic of the field can be well characterized by the Q-function, defined as, $Q(\gamma) = \frac{1}{\pi}\langle\gamma|\rho_r|\gamma\rangle$, where $|\gamma\rangle$ is the coherent state with a complex amplitude γ. The resonator's Q-functions, measured for quench times t = 0, 2.0, 2.5, and 2.8 μs, are displaced in Figure 1(a). As expected, the Q-function gradually evolves from the single- to double-peak structure during the quenching process. Each of these two peaks corresponds to a quasi-classical state with a broken symmetry, manifested by the nonzero phase-space coordinates of the local maxima, α_+ and α_-, which can serve as the order parameter [40]. The two peaks correspond to quasi-classical coherent states $|\pm\alpha\rangle$ with complex amplitudes $\pm\alpha$.

The two-peak pattern represents a signature of the second-order phase transition without coexistence of the normal and superradiant phases. This phase transition is in distinct contrast with the first-order SPT that features emergence of three peaks [41], one of which corresponds to the NP that coexists with the two SP components, as demonstrated in the previous experiment [22]. This significant distinction is mainly due to the fact that the control parameter ξ is linearly increased in the present experiment, but scaled in a highly nonlinear manner in the previous experiment. Due to the limitation of the experimental frequency ratio, $\Omega/\delta = 10$, the photon number does not show a divergent behavior at the critical point $\xi = 1$, corresponding to $t = 0.75$ μs, as shown in Figure S3 in Supplementary Material. This is due to the fact that the strongly squeezed resonator state, predicted to emerge near the critical point for the infinite frequency ratio [39], does not appear in the experiment.

Figure 1(b) displays the measured $|\alpha_+|$ (dots) and $|\alpha_-|$ (triangles) versus time. Due to the experimental imperfections, there is a certain degree of unbalance between the two degenerate ground states, which is continually enlarged when the control parameter ξ is increased. Due to the experimental imperfections, after the time $t \simeq 2.0$ μs $|\alpha_+|$ and $|\alpha_-|$

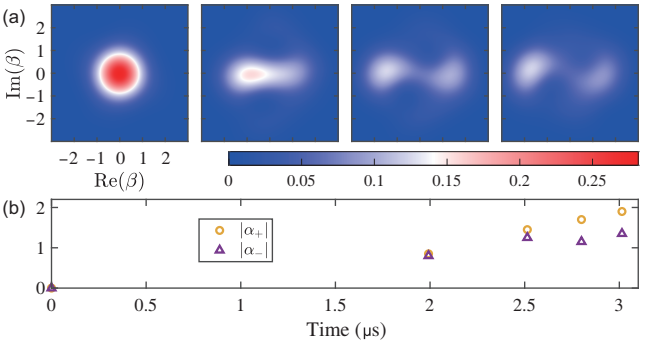

Figure 1 (Color online) Observation of phase-space evolution during the SPT. (a) Q-functions, measured for quench times t = 0, 2.0, 2.5, and 2.8 μs. During the process, the quench parameter as a function of time is modeled as $\xi = 0.5 + 2t/(3\ \mu\text{s})$. After the interaction between the test qubit and the resonator is effectively switched off, the resonator state is read out by subsequently performing a phase-space translation to the resonator, resonantly coupling it to an ancilla qubit, and recording the Rabi signals of the ancilla. (b) Phase-space coordinates of the local maxima, α_+ and α_-, versus quench time.

become inconsistent with each other and the discrepancy is continually enlarged. This discrepancy manifests the explicit symmetry breaking owing to the deviation of the realized Hamiltonian dynamics from the ideal symmetric case, which, however, does not destroy the quantum coherence between the two superimposing ground states. This discrepancy, as well as the unbalanced populations of these two components, manifests the explicit symmetry breaking owing to the deviation of the realized Hamiltonian dynamics from the ideal symmetric case, which is beyond the scope of the present work. We here focus on the SSB process where one of the two growing coherent states is singled out as the classical reality by the environment, which continuously gathers the information about which classical state the system is in, thereby deteriorating the quantum coherence that makes the two classical states suspending. The Q-functions of the resonator do not manifest the quantum coherence between the classical components. To obtain full information about this nonclassical behavior, it is necessary to perform a joint qubit-resonator state tomography.

The information of the field state associated with the qubit state $|j\rangle$ ($j = g, e$) is contained in the corresponding Wigner function, defined as:

$$\mathcal{W}_j(\beta) = \frac{2}{\pi P_j} \sum (-1)^n P_{j,n}(\beta), \tag{3}$$

where $P_{j,n}(\beta) = \langle j, n|D(-\beta)\rho D(\beta)|j, n\rangle$, and P_j is the probability of detecting the qubit in $|j\rangle$-state. Here the symbol "n" denotes the photon number in the resonator. These matrix elements are extracted by detecting the test qubit, and correlating the measurement outcome to the Rabi oscillation signals of the ancilla qubit resonantly coupled to the resonator following a displacement operation $D(-\beta)$ [22,42,43]. Figure 2(a) shows the conditional Wigner function, $\mathcal{W}_e(\beta)$, measured after quench times t = 2.5, 2.8, and 3.0 μs. The results clearly reveal a progressive loss of the quantum coherence between the two classical components, manifested by the gradual washing-out of the interference fringes between the two Gaussian-like peaks. Such a process can be understood in terms of the competition between the symmetric Hamiltonian dynamics and naturally-occurring dissipation, which continuously leaks the phase information about the growing field to the environment [10, 11]. This natural information acquisition accounts for coherence loss between the two suspending classical states, which leads to the SSB during the quantum phase transition. Due to the imperfect Hamiltonian control, the two Gaussian peaks are gradually diffused during the quench, which limits the size of the accessible output coherent field. The observation of the SSB can be pushed to a larger size with a more deliberately designed and fabricated device. The other conditional Wigner function $\mathcal{W}_g(\beta)$ measured exhibits a similar evolution behavior, as shown in Figure 2(b). In all the displayed Wigner functions, the main interference fringes appear in a region around the origin, which agrees with the numerical simulation presented in Figure S6. It should be noted that the measured Q-functions and Wigner functions present symmetric structures even for a classical mixture, which can be interpreted as follows. For each experimental implementation, one of the two symmetry-breaking classical states, but not both, is singled out as the reality. The symmetry of the phase-space distribution associated with such a classical mixture reflects that the two conflicting classical realities appear with the same probability.

Previously, the decoherence processes of Schrödinger-cat-like quantum superpositions have been demonstrated in cavity QED [44, 45], ion-trap [46] and mechanical resonators [47], where the cat states were pre-prepared, following which the decoherence effects were observed. However, in reality, the environment is always playing its role, instead of waiting to set in until the cat state has grown up. Our experiment illustrates such a process, where the parity symmetry is broken as a consequence of the competition between the unitary breeding of the cat state and the environment-induced dissipation. Such a competition is critical to the emergence of the classical reality from a quantum world, but has not been experimentally reported so far. Our results reveal that decoherence is responsible for breaking the symmetry inherent in the Hamiltonian dynamics.

The symmetry-breaking process can be further characterized by the evolution of the nonclassical volume [48], defined as the phase-space integral of the quasi-probability distribution over the regions with negative values. The nonclassical volume of the field state associated with the qubit state $|j\rangle$ is calculated as $\mathcal{V}_k = \left(1 - \int \mathrm{d}^2\,\beta\,|\mathcal{W}_k(\beta)|\right)/2$ which quantifies the quantum coherence between the two classical components. Figure 3 displays $\mathcal{V}_e$ and $\mathcal{V}_g$, inferred from

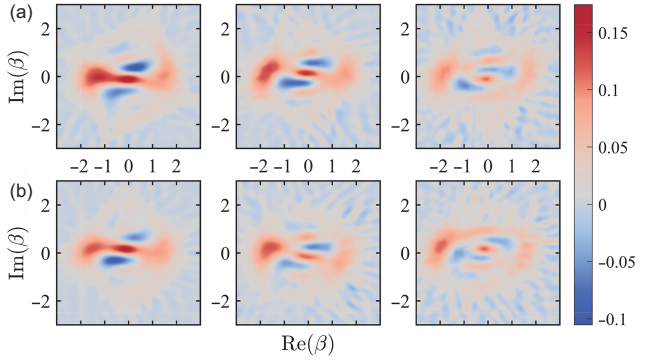

Figure 2 (Color online) Observation of the loss of the quantum coherence. (a) Wigner functions associated with the qubit state $|e\rangle$, measured after quench times t = 2.5, 2.8, and 3.0 μs. The results are obtained by correlating the Wigner function of the resonator to the measurement outcome $|e\rangle$ of the test qubit. (b) Measured Wigner functions associated with the qubit state $|g\rangle$.

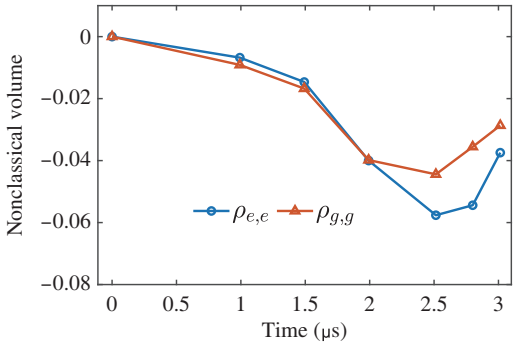

Figure 3 (Color online) Measured nonclassical volumes ($\mathcal{V}_k$) for different quench time. The nonclassical volume of the resonator's output state associated with the qubit state $|k\rangle$ ($k = e, g$) is defined as the integral of the corresponding Wigner function $\mathcal{W}_k(\beta)$ over the regions in phase space where $\mathcal{W}_k(\beta)$ is negative. As the negativity is a consequence of the phase-space quantum interference between the two classical components, the evolution of $\mathcal{V}_k$ manifests the process during which how the quantum coherence grows and then drops under the competition between the Hamiltonian dynamics and decoherence.

the Wigner matrices reconstructed for different quench times. When the phase-space separation between $|\alpha_\pm\rangle$ is small, the unitary dynamics dominate over the environment-induced decoherence, so that the quantum coherence is improved with the quench time. With the growth of the photon number, the cat state becomes increasingly vulnerable to decoherence. Finally, decoherence plays a dominant role, destroying the quantum coherence between the two classical components, and manifesting SSB.

5 Conclusion

In conclusion, we have observed the spontaneous symmetry-breaking process in the second-order phase transition, realized with an effective Rabi model synthesized in a superconducting circuit. With a high level of control over the system parameters, we move the system from the NP to a SP with two symmetry-breaking classical components, each corresponding to a photonic coherent state with a well-defined amplitude and phase. We monitor the SSB process, during which one of these two components is singled out as the classical reality. The results build a close relationship between SSB and environment-induced decoherence. With the improvement of the coherence times of the system, a SSB process can be observed with a larger cat size, which would shed new light on the quantum-to-classical transition.

This work was supported by the National Natural Science Foundation of China (Grant Nos. 11874114, 12274080, and 11875108), and the Innovation Program for Quantum Science and Technology (Grant No. 2021ZD0300200).

Conflict of interest The authors declare that they have no conflict of interest.

Supporting Information

The supporting information is available online at http://phys.scichina.com and https://link.springer.com. The supporting materials are published as submitted, without typesetting or editing. The responsibility for scientific accuracy and content remains entirely with the authors.

1 S. Sachdev, *Quantum Phase Transitions*, 2nd ed (Cambridge University Press, Cambridge, 2011).
2 Y. Nambu, Rev. Mod. Phys. **81**, 1015 (2009).
3 S. Weinberg, Eur. Phys. J. C **34**, 5 (2004).
4 J. Bardeen, L. N. Cooper, and J. R. Schrieffer, Phys. Rev. **108**, 1175 (1957).
5 J. Bernstein, Rev. Mod. Phys. **46**, 7 (1974).
6 F. Fumarola, B. Hein, and K. D. Miller, Phys. Rev. X **12**, 031024 (2022).
7 T. W. B. Kibble, Phys. Rep. **67**, 183 (1980).
8 J. van Wezel, J. van den Brink, and J. Zaanen, Phys. Rev. Lett. **94**, 230401 (2005).
9 J. Dziarmaga, W. H. Zurek, and M. Zwolak, Nat. Phys. **8**, 49 (2012).
10 L. P. García-Pintos, D. Tielas, and A. del Campo, Phys. Rev. Lett. **123**, 090403 (2019).
11 W. H. Zurek, Phys. Today **44**, 36 (1991).
12 E. Schrödinger, Naturwissenschaften **23**, 807 (1935).
13 M. Liu, D. A. Powell, I. V. Shadrivov, M. Lapine, and Y. S. Kivshar, Nat. Commun. **5**, 4441 (2014).
14 P. Hamel, S. Haddadi, F. Raineri, P. Monnier, G. Beaudoin, I. Sagnes, A. Levenson, and A. M. Yacomotti, Nat. Photon. **9**, 311 (2015).
15 Q. T. Cao, H. Wang, C. H. Dong, H. Jing, R. S. Liu, X. Chen, L. Ge, Q. Gong, and Y. F. Xiao, Phys. Rev. Lett. **118**, 033901 (2017).
16 G. Xu, A. U. Nielsen, B. Garbin, L. Hill, G. L. Oppo, J. Fatome, S. G. Murdoch, S. Coen, and M. Erkintalo, Nat. Commun. **12**, 4023 (2021).
17 B. Garbin, A. Giraldo, K. Peters, N. Broderick, A. Spakman, F. Raineri, A. Levenson, S. Rodriguez, B. Krauskopf, and A. Yacomotti, Phys. Rev. Lett. **128**, 053901 (2022).
18 M. L. Cai, Z. D. Liu, W. D. Zhao, Y. K. Wu, Q. X. Mei, Y. Jiang, L. He, X. Zhang, Z. C. Zhou, and L. M. Duan, Nat. Commun. **12**, 1126 (2021).
19 A. Safavi-Naini, R. Lewis-Swan, J. Bohnet, M. Gärttner, K. Gilmore, J. Jordan, J. Cohn, J. Freericks, A. Rey, and J. Bollinger, Phys. Rev. Lett. **121**, 040503 (2018).
20 M. Feng, Y. P. Zhong, T. Liu, L. L. Yan, W. L. Yang, J. Twamley, and H. Wang, Nat. Commun. **6**, 7111 (2015).
21 J. Fink, A. Dombi, A. Vukics, A. Wallraff, and P. Domokos, Phys. Rev. X **7**, 011012 (2017).
22 R. H. Zheng, W. Ning, Y. H. Chen, J. H. Lü, L. T. Shen, K. Xu, Y. R. Zhang, D. Xu, H. Li, Y. Xia, F. Wu, Z. B. Yang, A. Miranowicz, N. Lambert, D. Zheng, H. Fan, F. Nori, and S. B. Zheng, Phys. Rev. Lett. **131**, 113601 (2023).
23 J. Zhang, G. Pagano, P. W. Hess, A. Kyprianidis, P. Becker, H. Kaplan, A. V. Gorshkov, Z. X. Gong, and C. Monroe, Nature **551**, 601 (2017).
24 P. Jurcevic, H. Shen, P. Hauke, C. Maier, T. Brydges, C. Hempel, B. Lanyon, M. Heyl, R. Blatt, and C. Roos, Phys. Rev. Lett. **119**, 080501 (2017).
25 K. Xu, Z. H. Sun, W. Liu, Y. R. Zhang, H. Li, H. Dong, W. Ren, P. Zhang, F. Nori, D. Zheng, H. Fan, and H. Wang, Sci. Adv. **6**, 4935 (2020).
26 J. Klinder, H. Keβler, M. Wolke, L. Mathey, and A. Hemmerich, Proc. Natl. Acad. Sci. USA **112**, 3290 (2015).
27 Z. Zhiqiang, C. H. Lee, R. Kumar, K. J. Arnold, S. J. Masson, A. S. Parkins, and M. D. Barrett, Optica **4**, 424 (2017).
28 K. Baumann, C. Guerlin, F. Brennecke, and T. Esslinger, Nature **464**,

1301 (2010).
29 F. Brennecke, R. Mottl, K. Baumann, R. Landig, T. Donner, and T. Esslinger, Proc. Natl. Acad. Sci. USA **110**, 11763 (2013).
30 K. Baumann, R. Mottl, F. Brennecke, and T. Esslinger, Phys. Rev. Lett. **107**, 140402 (2011).
31 J. Léonard, A. Morales, P. Zupancic, T. Esslinger, and T. Donner, Nature **543**, 87 (2017).
32 J. Léonard, A. Morales, P. Zupancic, T. Donner, and T. Esslinger, Science **358**, 1415 (2017).
33 F. Ferri, R. Rosa-Medina, F. Finger, N. Dogra, M. Soriente, O. Zilberberg, T. Donner, and T. Esslinger, Phys. Rev. X **11**, 041046 (2021).
34 X. Zhang, Y. Chen, Z. Wu, J. Wang, J. Fan, S. Deng, and H. Wu, Science **373**, 1359 (2021).
35 L. Feng, O. Katz, C. Haack, M. Maghrebi, A. V. Gorshkov, Z. Gong, M. Cetina, and C. Monroe, Nature **623**, 713 (2023).
36 C. Chen, G. Bornet, M. Bintz, G. Emperauger, L. Leclerc, V. S. Liu, P. Scholl, D. Barredo, J. Hauschild, S. Chatterjee, M. Schuler, A. M. Läuchli, M. P. Zaletel, T. Lahaye, N. Y. Yao, and A. Browaeys, Nature **616**, 691 (2023).
37 S. Lloyd, Nat. Phys. **5**, 164 (2009).
38 S. Ashhab, Phys. Rev. A **87**, 013826 (2013).
39 M. J. Hwang, R. Puebla, and M. B. Plenio, Phys. Rev. Lett. **115**, 180404 (2015).
40 M. J. Hwang, and M. B. Plenio, Phys. Rev. Lett. **117**, 123602 (2016).
41 C. Zhu, L. Ping, Y. Yang, and G. Agarwal, Phys. Rev. Lett. **124**, 073602 (2020).
42 M. Hofheinz, H. Wang, M. Ansmann, R. C. Bialczak, E. Lucero, M. Neeley, A. D. O'Connell, D. Sank, J. Wenner, J. M. Martinis, and A. N. Cleland, Nature **459**, 546 (2009).
43 S. B. Zheng, Y. P. Zhong, K. Xu, Q. J. Wang, H. Wang, L. T. Shen, C. P. Yang, J. M. Martinis, A. Cleland, and S. Y. Han, Phys. Rev. Lett. **115**, 260403 (2015).
44 M. Brune, E. Hagley, J. Dreyer, X. Matre, A. Maali, C. Wunderlich, J. M. Raimond, and S. Haroche, Phys. Rev. Lett. **77**, 4887 (1996).
45 S. Deléglise, I. Dotsenko, C. Sayrin, J. Bernu, M. Brune, J. M. Raimond, and S. Haroche, Nature **455**, 510 (2008).
46 C. J. Myatt, B. E. King, Q. A. Turchette, C. A. Sackett, D. Kielpinski, W. M. Itano, C. Monroe, and D. J. Wineland, Nature **403**, 269 (2000).
47 M. Bild, M. Fadel, Y. Yang, U. von Lüpke, P. Martin, A. Bruno, and Y. Chu, Science **380**, 274 (2023).
48 A. Kenfack, and K. yczkowski, J. Opt. B-Quantum Semiclass. Opt. **6**, 396 (2004).